ESCUELA POLITÉCNICA NACIONAL

FACULTAD DE INGENIERÍA MECÁNICA

STUDY OF A DISTRIBUTED PROPULSION SYSTEM WITH BOUNDARY LAYER INGESTION IMPLEMENTED IN AN UNMANNED AERIAL VEHICLE, TO BE APPLIED IN THE ANDEAN REGION

TRABAJO DE TITULACIÓN PREVIO A LA OBTENCIÓN DEL TÍTULO DE INGENIERO EN INGENIERÍA MECÁNICA

SAÁ MADRIGAL JUAN MANUEL
juan.saa@epn.edu.ec

DIRECTOR: ING. VALENCIA ESTEBAN, Ph.D.
esteban.valencia@epn.edu.ec

CO-DIRECTOR: ING. HIDALGO VÍCTOR, D.Sc.
victor.hidalgo@epn.edu.ec

Quito, febrero 2018

CERTIFICACIÓN

Certificamos que el presente trabajo fue desarrollado por el señor **JUAN MANUEL SAÁ MADRIGAL**, bajo nuestra supervisión.

_____

Ing. Esteban Valencia, Ph.D.

DIRECTOR DEL PROYECTO

_____

Ing. Víctor Hidalgo, D.Sc.

CO-DIRECTOR DEL PROYECTO

DECLARACIÓN

Yo, **Juan Manuel Saá Madrigal**, declaro bajo juramento que el trabajo aquí descrito es de mi autoría; que no ha sido previamente presentado para ningún grado o calificación profesional; y, que he consultado las referencias bibliográficas que se incluyen en este documento.

A través de la presente declaración cedo mis derechos de propiedad intelectual correspondiente a este trabajo, a la Escuela Politécnica Nacional, según lo establecido por la Ley de Propiedad Intelectual, por su Reglamento y por la normativa institucional vigente.

_____

Juan Manuel Saá Madrigal

DEDICATORIA

A mis padres, a mis Alegrías, y abuelos. Por estar siempre en los mejores y peores momentos de mi vida.

AGRADECIMIENTO

A Dios por darme fuerzas para continuar día a día. A todas las personas que de una u otra forma me ayudaron en la consecución de este título, en especial a mi madre por apoyarme en todas mis decisiones y formarme como persona. A mi esposa y a mi hija por su amor incondicional y por ser mi soporte. A Galo, Maritza, doña Gladys y María Paz por la ayuda brindada. A mis abuelos por darme las bases de una buena formación. A doña Sixta y Antonio por el apoyo brindado en los últimos años de carrera. En general a todos mis amigos y profesores que han pasado por mi vida, porque de una u otra forma conocerlos me llevó al lugar en donde me encuentro.

A todos ustedes, gracias totales.

INDEX

NOMENCLATURE AND ABBREVIATIONS

BLI	Boundary layer ingestion
DP	Distributed propulsion/ Design point
UAS	Unmanned aerial system
UAV	Unmanned aerial vehicle
BWB	Blended Wing body
SSM	Systems for site specific monitoring
TS	Thrust split
C_L	Lift coefficient
C_D	Drag coefficient
C_{Do}	Zero lift Drag coefficient
M	Mach number
Re	Reynolds number
R	Ratio of specific heats for air
ρ	Air density
t_{amb}	Static temperature
T_{amb}	Total temperature
p_{amb}	Static pressure
P_{amb}	Total pressure
a_{amb}	Ambient sound velocity
$\dot{\boldsymbol{m}}$	Mass Flow
$\boldsymbol{n_f}$	Fan efficiency
$\boldsymbol{n_p}$	Propulsive efficiency
$\Delta \boldsymbol{P_{in}}$	Intake pressure losses
F_N	Thrust required
PW	Power required
TQ	Torque required
$\boldsymbol{V_\infty}$	Free stream Air velocity
$\boldsymbol{V_0}$	Air velocity at the intake
$\boldsymbol{V_j}$	Air velocity at the fan exit

RESUMEN

Las numerosas aplicaciones de vehículos aéreos no tripulados (UAV's) que vuelan a baja velocidad con fines de monitoreo en la región andina han motivado la investigación y evaluación de conceptos más eficientes, con el fin de mejorar su carga útil y alcance. En este contexto, se han estudiado conceptos de propulsión alternativos que presentan una mayor sinergia con los sistemas eléctricos. En un trabajo previo, se evaluó una configuración preliminar con propulsión distribuida usando un avión de cuerpo de ala mezclado (BWB) utilizando un análisis paramétrico. A partir de este estudio, las pérdidas de presión de entrada afectan en gran medida el rendimiento del propulsor. Este trabajo tiene como objetivo refinar el modelo desarrollado previamente para la evaluación del rendimiento de propulsión distribuida utilizando diferentes enfoques para las pérdidas de presión de entrada del modelo. Para este propósito, se utilizaron las correlaciones semiempíricas para el flujo incompresible, que relacionan la geometría del ducto con las características de flujo para calcular el coeficiente de fricción de la entrada. Además, se ha evaluado la idoneidad de implementar la ingestión de capa límite (BLI) con división de empuje sobre la configuración de propulsión distribuida. El caso de estudio tiene lugar en la región andina y, por lo tanto, la altitud de crucero para el estudio se ha establecido a 3000 m sobre el nivel del mar. Los resultados preliminares muestran que las pérdidas de ingesta basadas en los enfoques tomados son pequeñas para el caso de configuraciones sin BLI. Sin embargo, en el caso de BLI, donde se necesitan configuraciones de consumo más sofisticadas para reorganizar el flujo, el modelo actual no puede capturar su rendimiento. En el caso de BLI y empuje dividido se examinó su espacio de diseño. Desde este análisis, se encontraron mejoras de alrededor del 0,2% en la eficiencia de propulsiva y un aumento en la potencia consumida del 19% por la distorsión debido a la implementación de BLI.

Palabras clave: Ingestión de capa límite BLI, DP de propulsión distribuida, TS de empuje dividido, UAS de sistema aéreo no tripulado, UAV de vehículo aéreo no tripulado, Eficiencia propulsiva.

ABSTRACT

The numerous applications of unmanned aerial vehicles (UAV's) flying at low speeds for monitoring purposes in the Andean region have motivated the investigation and evaluation of more efficient concepts, in order to enhance their payload and range. In this context, alternative propulsion concepts that offer higher synergy with electrical systems have been studied. In a previous work, a preliminary configuration with distributed propulsion using a blended wing body (BWB) aircraft was assessed using a parametric analysis. From this study, intake pressure losses greatly affect the propulsor's performance. This work aims to refine the model developed previously for distributed propulsion performance assessment using different approaches to model intake pressure losses. For this purpose, semi-empirical correlations for incompressible flow, were utilized, which relate the duct geometry with flow characteristics to calculate the intake friction coefficient. Furthermore, the suitability of implementing boundary layer ingestion (BLI) with thrust split over the distributed propulsion configuration has been evaluated. The case of study takes place in the Andean region and hence the cruise altitude for the study has been set at 3000 m above sea level. Preliminary results show that the intake losses based on the taken approaches are small for the case of no BLI configurations. However, in the case of BLI, where more sophisticated intake configurations to re-arrange the flow are needed the current model is not able to capture their performance. In the case of BLI and thrust split their design space was examined. From this analysis improvements of around 0,2% in propulsive efficiency and a increase in power consumed of 19% due to distortion because of BLI implementation were found.

Keywords: Boundary layer ingestion BLI, Distributed propulsion DP, Thrust Split TS, Unmanned aerial system UAS, Unmanned aerial vehicle UAV, Propulsive efficiency.

STUDY OF A DISTRIBUTED PROPULSION SYSTEM WITH BOUNDARY LAYER INGESTION IMPLEMENTED IN AN UNMANNED AERIAL VEHICLE, TO BE APPLIED IN THE ANDEAN REGION

INTRODUCTION

The economy of Andean countries such as: Ecuador, Colombia, Chile, Peru and Bolivia; have depended historically on the agricultural sector, which for its technification presents several challenges due to the complexity of their topology. Agriculture takes an important share of each country's GDP and hence governmental efforts have been implemented to technify it and enhance agricultural production. For instance, Ecuador has set the "Plan Nacional del Buen Vivir" (PNBV) framework [1] to set policies to achieve production targets in terms of agricultural production. Nevertheless, the suitability of these systems for site specific monitoring (SSM) depends highly on the improvements in performance that can be achieved in order to increase their payload and range for high altitude monitoring (above 3000 m). In the case of Ecuador, crops requiring SSM account for 1200 km2 [2] which would represent approximately 60 trips with current commercial UAVs (unmanned aerial vehicles) platforms [3] since SSM requires data collection several times per month depending on the type of crop the above mentioned figure constraints up to certain extent its implementation in the field. This one has motivated the search of novel low cost UAS (unmanned aerial systems) with high performance at high altitudes. Being the propulsion system the "heart" of aerial systems, the aforementioned panorama requires a breakthrough in current technology to enable efficient electrical power-propulsion systems. UAVs present less design constrains compared with other aviation sectors, due to their unmanned features, which have enabled a fast pace of innovation.

Based on a previous work [4] where distributed propulsion was examined for a sUAS concept applied for precision agriculture, this work seeks to refine the models developed for the calculation of intake pressure losses, which was found as a main aerodynamic integration issue in the implementation of distributed propulsion systems. Another important technology to improve thermal and propulsive efficiencies is BLI (boundary layer ingestion) [5] due to its high synergy with BWB (blended wing body) and distributed propulsion [6], this has been implemented in the current distributed propulsion analysis. Finally, to search novel propulsion configurations the thrust split between the distributed propulsors is investigated. In the following paragraphs further description of BWB airframe, propulsion system technologies and integration aspects are presented.

Research question

Is it possible to implement distributed propulsion with boundary layer ingestion on unmanned aircraft to high altitude conditions and climate of the Ecuadorian highlands?

General objective

Study of a distributed propulsion system with boundary layer ingestion implemented in an unmanned aerial vehicle to be applied in agricultural, medical and surveillance areas in the Andean region.

Specific Objectives.

- Determine a methodology and design space in the distributed propulsion systems.
- Develop preliminary configurations of distributed propulsion for unmanned aerial systems based on applications in the fields of agriculture, medicine and surveillance.
- Develop a parametric code to establish a "Thrust Split" configuration based on one main fan and one or more secondary fans.

1. THEORETICAL FRAMEWORK

The size and configuration of the aircraft plays a very important role in choosing the aircraft according to the applications in which it is intended to be used. The conventional configuration of the aircraft usually generates a large amount of drag because of the various control surfaces that it presents. In addition to that there is a large surface of the fuselage that does not help with the lift generation. The proposed configuration for this titling project is called the BWB (Blended Wing Body), that is a fixed wing aircraft that does not have a clear dividing line between the wings and the main body of the ship.

This form of aircraft allows the entire body to have an aerodynamic profile, pretending that the entire surface generate lift [7]. However, in civil aviation studies have shown that this type of aircraft can present stability problems due to the high speeds at which they operate, the great difference of pressures that this generates in the fuselage, the reduction of the control surfaces and the body-wing integration as in conventional aircraft [8]. Despite this, it is expected that, for relatively small-sized unmanned aircraft compared to those used in civil aviation, these stability problems will not occur as they fly at much lower speeds and heights, resulting in differences in fuselage pressures of smaller proportion. On the other hand, due to the smaller dimensions, strong winds could generate significant problems of stability and control.

Distributed propulsion is a type of technology that has been implemented a few years ago especially in unmanned aircraft that use a vertical takeoff as in quadrupole. However, this type of takeoff generates a great energetic consumption. This type of propulsion has also begun to be studied in BWB aircraft hoping to obtain advantages in terms of weight distribution, reduction of propeller size, ease of transportation, among others. For civil aviation, the implementation of this technology presents a big problem in terms of pressure losses in the ducts of the propellers, which causes a great increase in the power required by the engines. In unmanned aircraft the pressure losses in the ducts are expected to be much lower than in civil aviation for different reasons such as: The shorter duct length (reduced contact area with airflow); the smaller velocity at which it is expected to fly.

Although the air flow is in a turbulent regime, the Reynolds number is much smaller, therefore the friction factor with the surface of the duct proves to be smaller, and the air flow at the intake would be able to rearrange in an easier way [4].

Boundary layer ingestion (BLI) is another type of technology that together with the distributed propulsion has the purpose of increasing the propulsive efficiency and decrease the energy consumption required by the engines. For the implementation of

BLI the propellants must be located within the aircraft, which entails certain challenges, especially the aspects of aerodynamic integration, which are related to the pressure losses in the duct of the propellers and the decrease of propellant performance due to distortions [9].

The present work will propose a configuration of the propellers in number, size and location within the fuselage of an aircraft, pretending to be a starting point for the solution of this research problem.

1.1. Aerodynamic assessment – BWB Airframe

The blended wing body airframe combines different airfoils for the wings and for the center body as well. The principal purpose of this configuration is to generate lift throughout the whole airframe, not only the wings [7]. This concept has been studied, by NASA and BOEING, as an alternative to the typical tube-and-wings configuration for massive transport obtaining a working prototype in 2007: the X-48B [7],[11], and in more recent research and a new NASA aircraft concept: the N3-X has been studied [12]. Figure 1.1 shows a perspective of these aircraft and a comparative lift/load distribution of BWB and a tube-wing configuration [7].

The studies performed by BOEING showed 15% reduction in TOW (take- off weight), with 27% reduction in energetic consumption for a BWB subsonic transport for 800 passengers [11]. These milestones were achieved due to the superior aerodynamic characteristics of the BWB for the fact that there are improvements in the distribution of the lift along the structure as shown in Figure 1.1 (c). The X-48B aircraft was a prototype developed to assess the suitability of BWB configurations in civil aviation [13]. Most of studies for BWB configurations are carried out at similar operating conditions as civil aircraft, and hence they are tested at high Reynolds and high Mach numbers ($Re > 2(10)^6$ and $M > 0.7$) in comparison with UAS for SSM. Since the Mach and Reynolds numbers are lower ($Re < 10^6$ and $M < 0.1$) for this application, studies carried out for similar conditions have been defined for the model validation. One study compatible for SSM applications is the one developed by Wisnoe [13] where two BWB configurations operating at 0.1 Mach number are studied experimentally. Since the information on both concepts was extensive and available in the open domain, one of these configurations (base line I) was selected for the propulsion performance analysis in a previous work[4]. Nevertheless, the baseline I concept presented low aerodynamic performance and hence for this study a design adapted from the one developed by Shim and Jo [14], [15] has been used. For this latter concept the cruise speed corresponds to 50 m/s. In figure 1.2 the views of the concept utilized are shown.

a) Nasa's X-48-B Aircraft [11] .

b) Nasa's N3-X Aircraft [10].

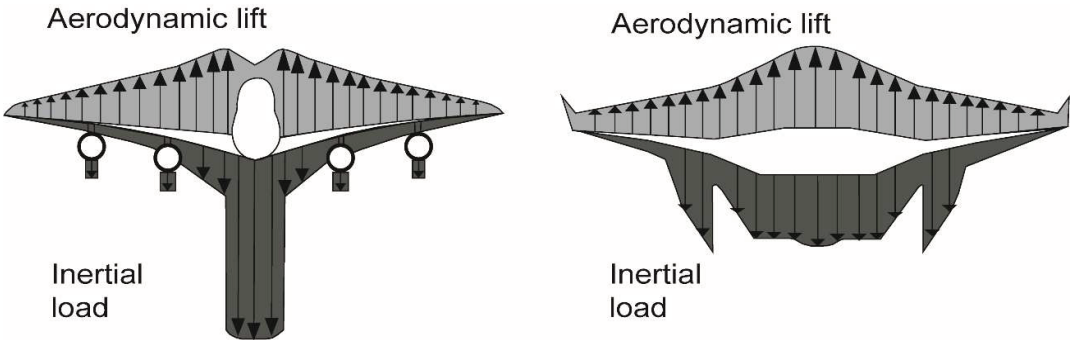

c) Lift and load comparison between a conventional aircraft and a BWB [7].

Figure 1.1. Airframe assessment.

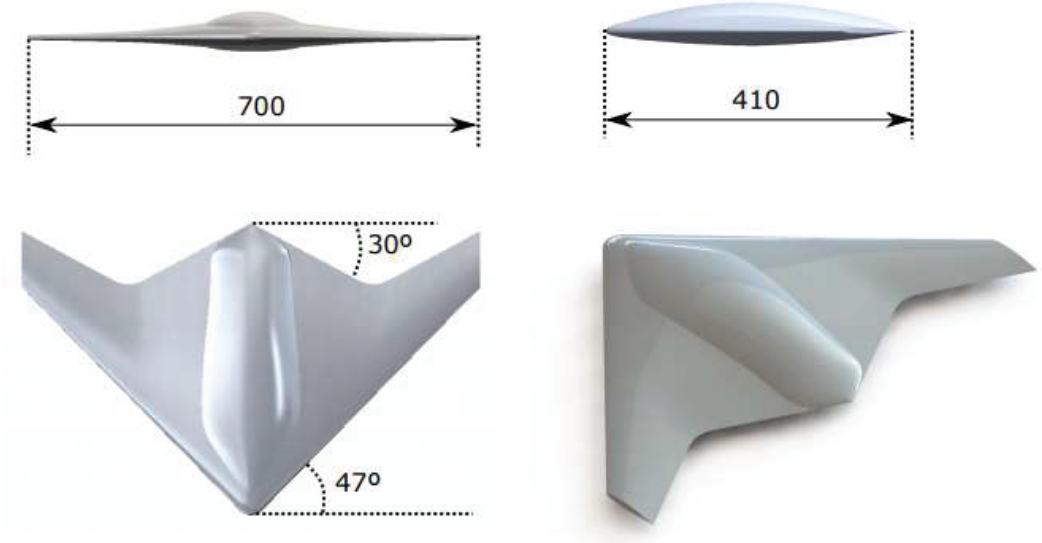

Figure 1.2. Four different views of BWB-UCAV model [14].

1.2. Propulsion system

UAVs implemented in SSM for agriculture usually are electrical powered, and their design is a multidisciplinary task, that considers: propulsion, transmission and electrical systems. In the work developed by Gur [16] the optimization of an electric propulsion system consisting on: propeller, electric motor and batteries; is carried out. However, this method focuses mainly on conventional propulsion architectures. The need of more efficient systems has motivated the searching of alternative propulsion designs. Specifically, for BWB airframe, distributed propulsion and boundary layer ingestion (BLI) have been explored with the aim of improving the payload and endurance of UAVs in the agricultural sector [4]. Although the aforementioned technologies have been explored for civil aviation [17], [18], [19] their suitability for electrical powered sUAS has not been fully examined.

1.2.1. Distributed propulsion system

Distributed propulsion (DP) systems with boundary layer ingestion (BLI) have been explored and documented extensively because of its potential benefits in terms of propulsive efficiency and energy consumption [20],[17],[21].

Distributed propulsion has been defined by H. Kim [22] as the span-wise distribution of the propulsive thrust stream in order to maximize the overall vehicle benefits in terms of aerodynamic, propulsive, structural, and/or other efficiencies. From the performance perspective, replacing the main engine's fans by a propulsor arrangement enables to achieve very high by pass ratios, without the fan size limitation [22], and hence contributes to improve the propulsive efficiency . The aforementioned DP performance features have been studied for distributed fans driven by gas turbines. However, in sUAS batteries replace gas turbines as energy source, and hence the performance benefits are expected to be mainly accrued from: i) aerodynamic performance, due to reduction in drag installation losses; ii) structural design, as it enables a better load distribution along the airframe; iii) safety/reliability, due to a large number of independent propulsors; iv) enabling technology, DP presents configuration synergies with thrust split and BLI as shown in figure 1.5. The work developed by Perry studies the behavior of a distributed propulsion system with BLI composed by 5 electric ducted fans. In which the results indicated non-linearities as a function of the angle of attack and acceleration, showing a different behavior depending on which were the operating fans, improving or decreasing their performance [23]. This result mean that the distortions caused by the size and quantity of the fans can increase according to their disposition and functioning.

For this reason, in this work the effect of the ingestion of the boundary layer, as well as possible problems of aerodynamic integration that will be explained later have been studied.

1.2.2. Boundary layer ingestion

The boundary layer ingestion (BLI) seeks to reduce the total power required by the propulsors, placing them inside the aircraft (totally or partially) where the boundary layer can be ingested and with it, a lower velocity of the air compared to the velocity in free stream. With the implementation of BLI, the wake produced by the aircraft undergoes a re-energization, which causes a reduction in the total wasted energy, allowing the aircraft to move with the same thrust with a lower power required by the propulsors. The equations from 1.1 to 1.4 detail the torque and power required by the thrusters for the two configurations (with and without BLI) for the cruise condition, where the thrust required by the propulsors is assumed equal to the drag generated by the fuselage. In addition, the drag produced by the propulsors and control surfaces is not taken into account for the present study. The complete deduction of the formulas used can be seen in [24].

The thrust required by the thrusters for each configuration is detailed in equations 1.1 and 1.2:

$$F_{N,\ no\,BLI} = \dot{m}_f \cdot (V_j - V_0) \tag{1.1.}$$

$$F_{N,\ BLI} = \dot{m}_f \cdot (V_j - V_{avg}) \tag{1.2.}$$

Where V_{avg} is the average velocity at the intake of the propulsor in the BLI configuration, V_j is the exit velocity of the fluid and V_0 intake velocity in free stream.

In equations 1.3 and 1.4 the power required for the podded configuration and with BLI respectively are detailed:

$$PW_{f,\ no\,BLI} = \frac{F_N}{2}(V_j + V_0) \tag{1.3.}$$

$$PW_{f,\ BLI} = \frac{F_N}{2}(V_j + V_{avg}) \tag{1.4.}$$

A lower momentum drag ($\dot{m}_f \cdot V_{avg}$), could represents benefits in terms of propulsive efficiency and energy consumption. Since V_{avg} is an average of the air velocity ingested, and is less than the V_0, it is evident that the power required by the propellers is lower in the case of BLI compared to the podded configuration, as seen in the equation shown above.

A fully embedded installation offers the opportunity to ingest a substantial part of the inboard boundary layer (15% of the bare airframe drag) and allows for a reduction in wetted area and structural weight because of the disappearance of pylons [25]. Nevertheless, BLI also brings some challenges, especially aerodynamic integration aspects, which are related to the intake pressure losses and fan performance detriment due to distortion.

The advantages of implementing BLI have been studied in conventional aircraft in research as the one done by Blumenthal where a comparison between the power required by conventional configuration and a mixed configuration (BLI and podded configuration) was carried out. Obtaining a reduction in power requirements between 14,4% and 15,6% at cruise for the BLI configuration over the baseline geometry as well as a drag reduction of approximately eighteen counts over the baseline geometry [24].

The intake pressure losses are linked to the complex duct design that embedded installations require [12]. On the other hand, the fan performance detriment is related to the combined radial and circumferential distortion caused by BLI [6]. Distributed propulsion systems with BLI in BWB airframe could bring a 15 % fuel burn saving relative to today's aircraft [26]. Another study shows benefits in terms of an increment overall fan efficiency about 3% with a BLI configuration in the D8 NASA aircraft [27]. However, these benefits might be overweight by aerodynamic integration issues, such as: distortion and intake pressure losses. Figure 1.3 shows a boundary layer ingestion scheme.

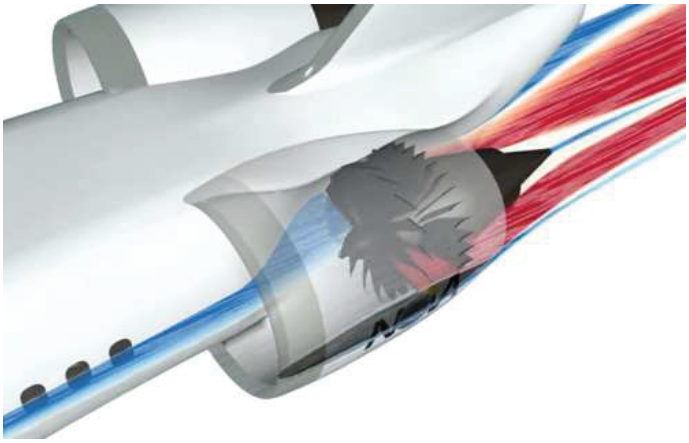

Figure 1.3. Boundary layer ingestion scheme [28].

1.3. Thrust Split

Thrust split is defined as the ratio of propulsor array thrust over the intrinsic net thrust [29]. Therefore, it includes another design parameter, which enables the searching of novel propulsion architectures. In this context, thrust split could bring benefits in different areas such as: structural design, control system, stability and reliability. Similarly, to distributed propulsion thrust split could benefit the UAS design by reducing the size of the distributed propulsor array and hence improve loading distribution in the structural design. For instance, to avoid excessive weight loads at the wing tips, thrust split could be used to define a main electric ducted fan at the body centerline, which produces a large part of the thrust, which could be useful in one engine off scenarios.The thrust split is defined through equation 1.5.

$$T_S = \frac{F_{SP}}{F_N} \tag{1.5.}$$

Where, F_N stands for the net thrust and the secondary propulsors thrust (F_{SP}) is defined by equation 1.6.

$$F_{SP} = \frac{F_N - F_{MP}}{NF} \tag{1.6.}$$

In figure 1.4 and 1.5 are shown schemes of thrust distribution for different cases of thrust split.

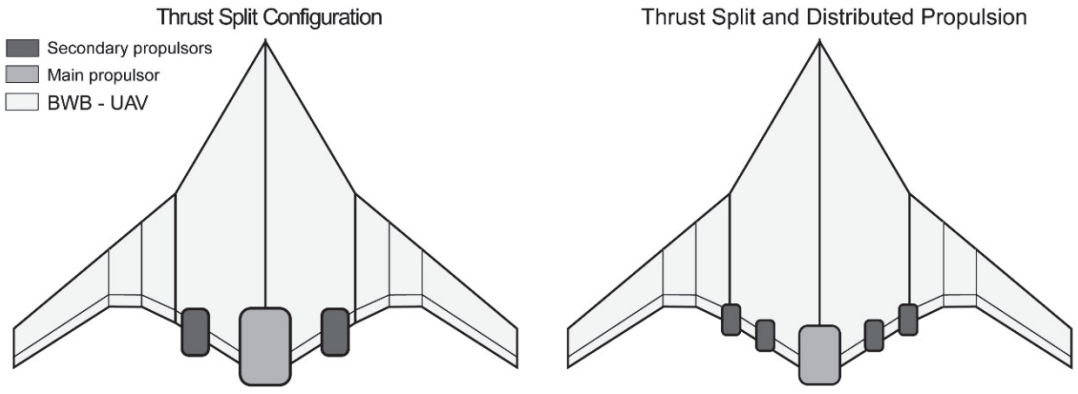

Figure 1.4. Thrust split scheme [30].

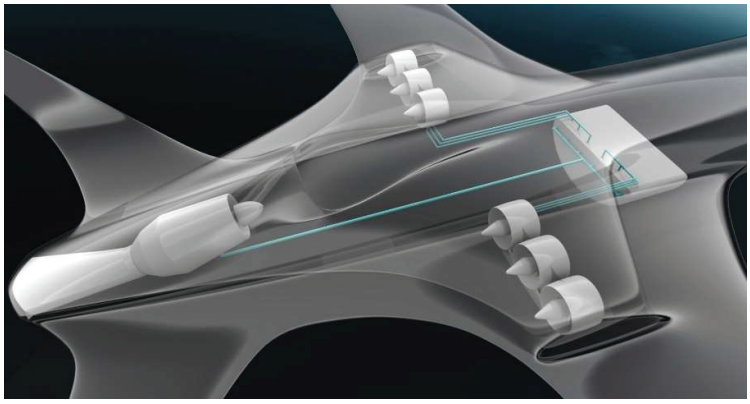

Figure 1.5. Thrust split scheme [31].

1.4. Airframe propulsion integration problems

The present work analyses the performance of a distributed propulsion system for a BWB configuration with a parametric method developed by Valencia [29]. This work investigated the effect of aerodynamic integration effects in highly coupled configurations as distributed propulsion with BLI. In this context, intake pressure losses and detrimental performance of the fans were assessed to define optimal configurations in terms of power consumption.

For the case of study, the operating conditions are based on the implementation of sUAS in the agricultural sector suitable for the Andean region (3000 (m)). Based on these optimal configurations a conceptual design was developed based on electric ducted fans available in the market. It is important to mention that because of availability the ducted fan and electrical engine combined set-up were selected for each of the optimal configurations.

1.4.1. Distortion

BLI propulsion systems are largely affected by the level of distortion in the inlet flow field, for instance combined distortion may cause 2 % detriment in fan efficiency [32] for civil aviation fans, which can be considerably larger for small turbomachinery due to the larger effect of losses over the performance of these latter [33]. Through flow methods [34] and parallel compressor [25] have been used to calculate the effects of this aerodynamic integration issue on the performance of the fans. High fidelity through flow methods are computationally expensive, and for that reason they are not convenient at a preliminary design stage. On the other hand, parallel compressor is able to assess only circumferential distortion.

The work developed by Valencia [35], introduces a discretized semi-empirical performance method, which uses empirical correlations for blade and performance calculations. This tool discretizes the inlet region in radial and circumferential directions enabling the assessment of deterioration in fan performance caused by the combined effect of both distortion patterns. This method presents the advantages of being versatile and low computational demanding, which make it suitable for conceptual and preliminary design.

Figure 1.6 shows the variation in the air Mach number passing throw an axial fan. In the blade tips the variation of the air properties is greater than in the rest of the blade. That´s why in smaller fans the distortion could cause a bigger reduction in the fan efficiency. In the present work, an experimental test was carried out to determine the fan efficiency of a commercial ducted fan in a BLI configuration [36].

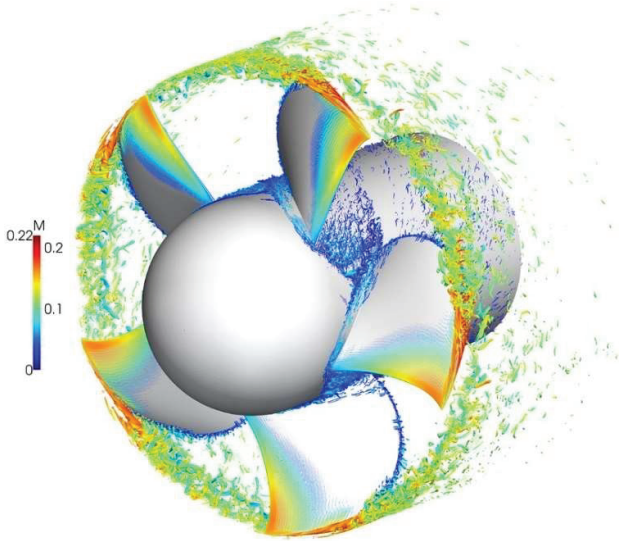

Figure 1.6. Instantaneous contours of the Q-criterion, colored by the relative Mach number, show the vorticial structures of the flow field [36].

1.4.2. Intake pressure losses

BLI requires a highly coupled configuration and hence the duct design is a cumbersome task, which needs to provide a high efficient diffusion whilst re-arranging the incoming flow. Previous works about BLI show that distributed propulsion systems are very sensitive to intake pressure losses [4], [29]. Research about duct design shows that with embedded s shape or irregular duct geometries increases the distortion, and a separation of the boundary layer may occur because of the pressure gradient in the duct [37], [38]. In ducts with conical inlets, a flow separation may occur depending on the angle selected and the Reynolds number considered [39]. This behavior of the flow is

not desirable because of distortion patterns that may cause large detriments in the fan performance due to the ingestion of non-uniform flow. Intake pressure losses in s-shaped ducts for BWB airframes implemented in civil aircraft account for 2% to 6% [18], [25], which is very high compared with current intake designs, as mentioned in Valencia [29], losses larger than 2% might overweight the benefits accrued from BLI. In a previous work [4], a preliminary design for a distributed propulsion system was explored and a configuration with three ducted fans was found as optimal. However, these optimistic results were based on lower than 2 % pressure losses. In order to refine this model, the present work included a parametric approach to define the intake losses based on the wetted area and incomming flow characteristics. This aspect is important to highlight, since most of the information regarding duct design focuses on s-shaped ducts and intakes for civil aviation, which have different geometrical constrains in comparison with the UAV sector. For the current research the model proposed by Jaurker [40] will be considered for the intake losses calculation, this model is selected due to its simplicity and its good agreement with experimental data.

1.4.3. Fan efficiency

The efficiency for large propellers used in civil aviation is around 85% due to their characteristics [21]. In small propulsors, such as those evaluated in the present work, the efficiency is above 70% [41], when there is no boundary layer ingestion. The fan efficiency is function of the fan pressure ratio (FPR), speed or temperature difference at the intake and exit of the fan. With BLI a decrease in the efficiency of the fans is expected, and this factor is determinant in the analysis of parameters like the power or torque required.

Ducted fans behave like compressors with low FPR. For satisfactory performance, the relative velocity at exit from a blade row should be at least 72% of the inlet relative velocity. This is similar to limit the pressure rise across each blade row and the maximum stage loading possible. The stage loading is defined as the ratio of the specific work (ΔW) change through a sage to the square of the blade speed (V_b) [33], as show in equation 1.7.

$$\varphi = \frac{\Delta W}{V_b^2} = \frac{\dot{m}\, c_p\, \Delta T}{V_b^2} \tag{1.7.}$$

Equation 1.8 shows a theoretical relationship between the stage loading and the flow coefficient. The flow coefficient is defined as the ratio of the meridional flow velocity to the blade speed, equation 1.7. For higher values of flow coefficient correspond higher

inlet mass flow per unit areas, which represents an advantage as it implies a smaller diameter propoulsor for a given mass flow. The change on performance is higher at very low flow coefficients, where high incidence can also lead to flow separations [33]. Figure 1.7 shows a comparison of simplified analysis with measured performance of a compressor stage.

$$\varphi = 1 - 0.438\emptyset \tag{1.8.}$$

$$\emptyset = \frac{V_\infty}{V_b} \tag{1.9.}$$

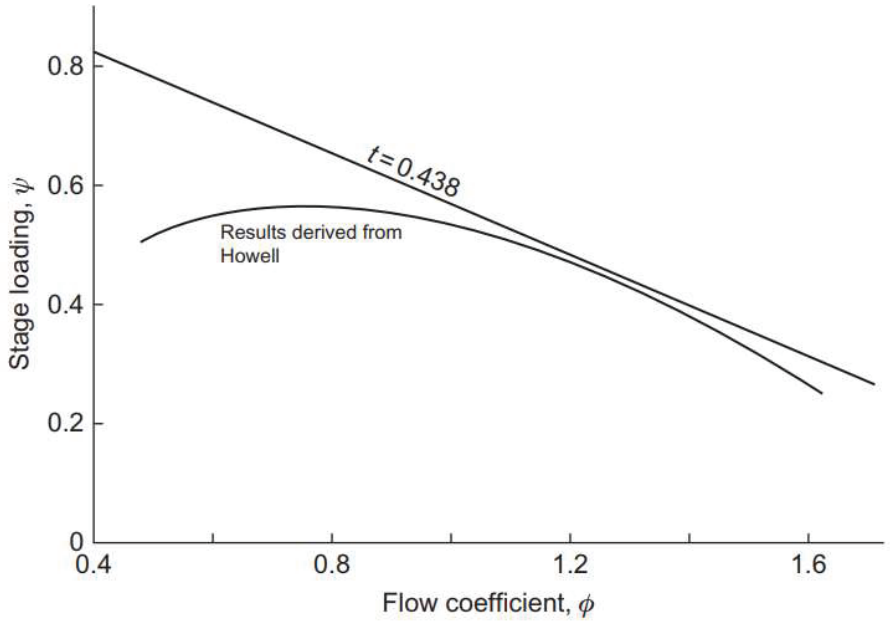

Figure 1.7. Compressor stage performance: comparison of simplified analysis with measured performance [33].

To summarize, this work refines previous models [4] for the boundary layer characterization and for the assessment of intake pressure losses. Through this, the performance of distributed propulsion systems with BLI is examined. Furthermore, a design space variable denominated thrust split has been included in the analysis to achieve a non-homogeneous thrust distribution. The study case in this work is a sUAS used for precision agriculture and monitoring tasks suitable for the Andean region (3000 (m)).

2. METHODOLOGY

In this section, the method utilized to assess the propulsion and aerodynamic performance of the small UAS for precision agriculture is explained. In figure 2.1 a schematic representation of the calculation process is presented and as indicated, the process can be summarized by the following calculation modules: i) aerodynamic characteristics and operating conditions, ii) aerodynamic data at design point (cruise or loitering phases), and iii) propulsion system performance.

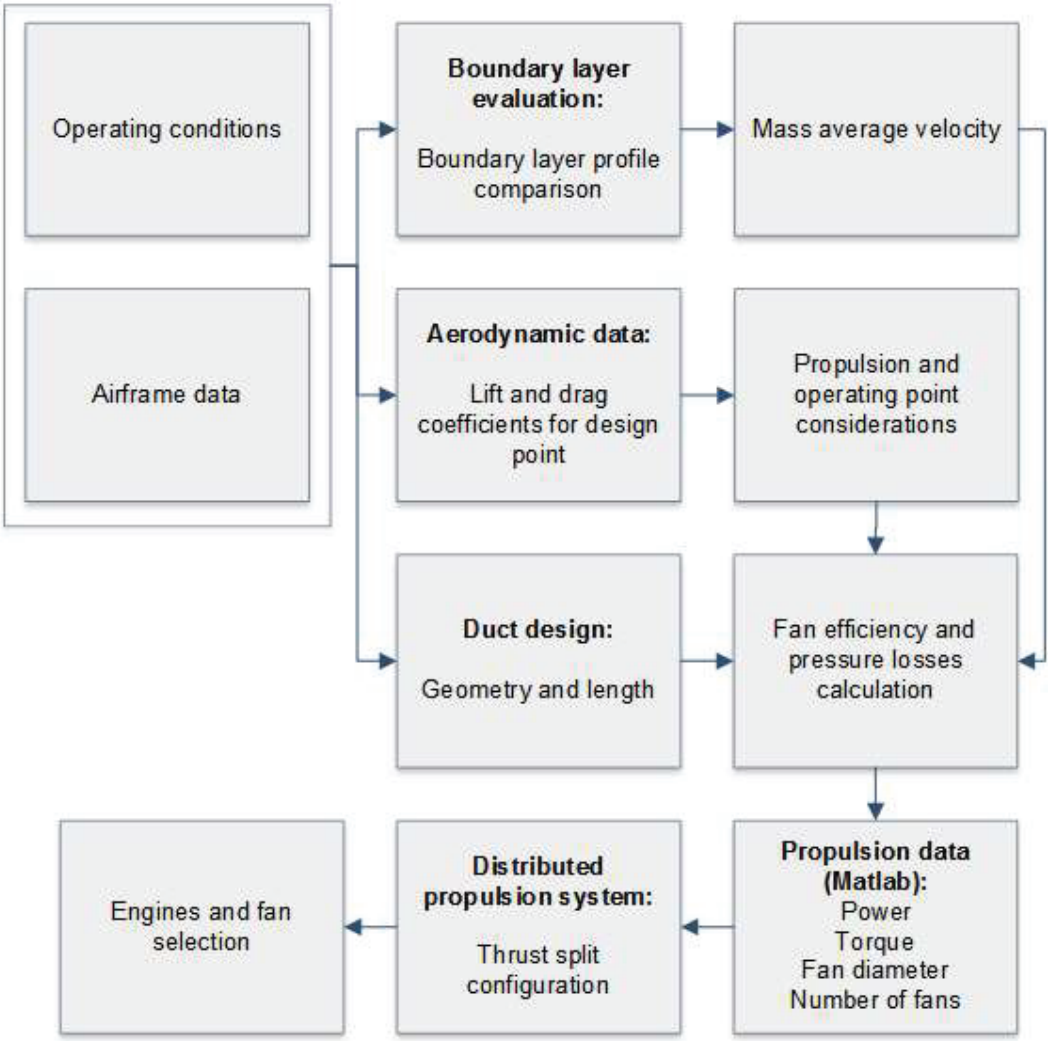

Figure 2.1. Methodology stages.

2.1. Base line configurations and operating conditions

As mentioned previously the baseline airframe configuration was selected from a geometry adapted from the work of Shim and Jo [14], [15], for this geometry the aerodynamic characterization is explored in Hidalgo [6]. Since the current analysis is carried out at design point, the operating conditions assumed were: 3000 m above sea level, which suits most of crops in the Andean region for SSM and also complies with local regulations for sUAS [42].

The flight velocity at cruise condition is set at Mach number 0,1, which is based on the payload restrictions for SSM. Figure 1.2 shows the baseline airframe configuration.

2.2. Aerodynamical model

An important input parameter in the propulsion system module is the intrinsic net thrust, which for steady, symetrical, non-acelerated flight is assumed equal to the drag of the aircraft. To estimate the drag of the aircraft a basic parametric approach based on the parabolic drag polar approximation has been used. Equations 2.1, 2.2 and 2.3 are used to calculate the aircraft drag for the best endurance case [43], which is assumed as the design point condition.

$$C_{LE} = \sqrt{3 \cdot C_{Do} \cdot \pi \cdot AR \cdot e} \tag{2.1.}$$

$$C_{DE} = C_{Do} + \frac{C_{LE}^2}{\pi \cdot AR \cdot e} \tag{2.2.}$$

$$D = \frac{1}{2} C_{DE} \cdot \rho \cdot V_\infty^2 \cdot S \tag{2.3.}$$

In table 2.1 is described the airframe baseline data.

Table 2.1. Airframe and aerodynamic data

$S\ (m^2)$	$b\ (m)$	AR	C_{Do}	C_L	α	e
0,127	0,7	3,85	0,00842	0,5	0°	0,685

For the sake of simplicity, the drag calculated at this stage corresponded to the clean airframe, without considering the drag from auxiliary components such as: wheels, cameras, antenas, compartment doors, wires, which will be considered in future research. Furthermore, the drag variation due to different propulsion configurations will

not be considered for the analysis. Since the propulsion system is analyzed using an internal control volume which encompassess only the distributed propulsors. This aspect is further explained in the next section.

2.3. Propulsion system modeling

For the modelling of the electric ducted fan the same methodology described in Valencia [21] is utilized. Based on this an internal control volume approach, which encloses the distributed propulsors and accounts for the BLI benefit from the momentum drag reduction is implemented in further analysis [18], [21]. This approach only includes in the analysis the propulsor, neglecting the airframe and its wake.

For the sake of simplicity only the centreline propulsor is analyzed and this is asumed to be located at 0.75 of the centerline chord. The spanwise effects have not been considered and the precompression region is neglected. Furthermore, the total aircraft drag is considered constant for all the configurations and hence the benefit only comes from the inlet momentum drag reduction. It is important to note that the only change in aircraft drag that should be added will be related to the change in geometry of the distributed propulsion section, however for this preliminary design stage the change of wetted area does not alter the results considerably.

Figure 2.2 shows the podded and BLI configurations, where the embedding region is shown. In the weight analysis for the propulsors the embedding region (%NE) is considered to define the location of the propulsor over the airframe [30].

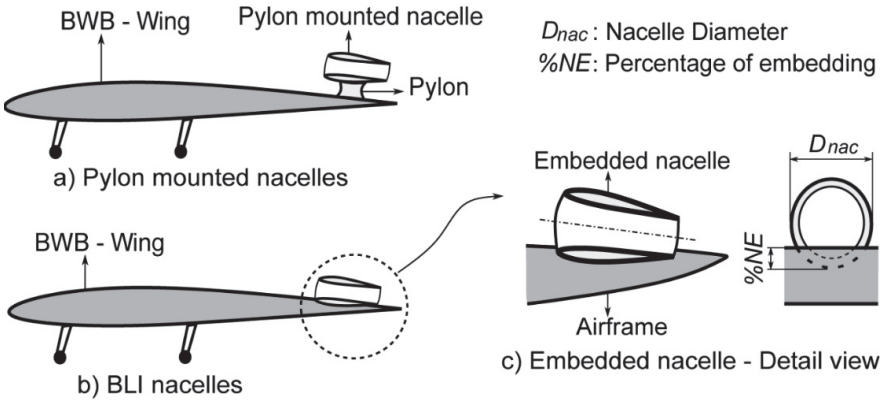

Figure 2.2.Podded and BLI configurations [30].

2.3.1. Distributed propulsion system

For the assessment of the propulsion performance the parametric approach [14] made several assumptions in order to simplify the analysis. Firstly, the inner control volume approach [18] shown in figure 2.3 was utilized (the control volume encloses only the propulsor) for the calculation of the propulsor's mass flow determined by the thrust requirement. In this control volume, the pre-compression zone was not considered and hence the inlet of the control volume was assumed at the same station as the propulsor inlet. Furthermore, the drag installation losses and nacelle drag variation due to the propulsor's size was not considered.

Although the latter is important in the propulsion performance assessment, at this stage of the preliminary design this effect was neglected.

In future work this feature will be implemented in the methodology, so the trend presented in this work can be refined. In order to calculate the fan inlet and outer diameter the present work assumed a hub to tip ratio of 0,056, which is conventional for electric ducted fans [44].

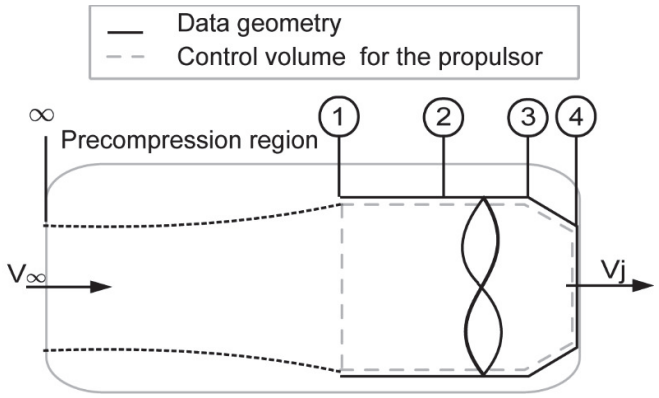

Figure 2.3. Inner control volume for the podded installation case [4].

Using the drag calculated with the aerodynamic module based on the best endurance case and for the cruise condition assumed, drag equals to lift and hence the propulsor's mass flow can be calculated. The parametric code developed first calculates the different parameters for the height selected. Such as the ambient total and static temperature, pressure, the density and Mach number according to the next equations.

$$t_{amb} = 288{,}15 - 0{,}0065 \cdot H \tag{2.4.}$$

$$p_{amb} = 101325 \cdot (1 - 0.0000226 \cdot H)^{5{,}256} \tag{2.5.}$$

$$a_{amb} = (r \cdot R \cdot t_{amb})^{0.5} \tag{2.6.}$$

$$T_{amb} = t_{amb} \cdot \left(1 + M^2 \cdot \frac{r-1}{2}\right) \tag{2.7.}$$

$$P_{amb} = p_{amb} \cdot \left(1 + M^2 \cdot \frac{r-1}{2}\right)^{r/(r-1)} \tag{2.8.}$$

With this data, the Drag is calculated as shown previously (equation 2.3) and is equal to the thrust required, as explained previously. The mass flow and the velocity for the intake and the exit fan are calculated and then the mass flow fan and power required can be determined. Taking the engine as the reference, the air enters the intake with a velocity V_0 relative to it. V_0 is equal and opposite to the speed of the aircraft.
The air is accelerated and it leaves with the propulsor with velocity V_j. The mass flow $\dot{m}$ is assumed constant and thus the net thrust F_N due to the rate of change of momentum is explained in equation 1.1 [45].

Where mV_j is called the gross momentum thrust and mV_0 the intake momentum drag. Therefore, the mass flow and the power required are determined by the next equations:

$$\dot{m}_f = \frac{F_N}{V_j - V_0} \tag{2.10.}$$

$$PW_f = C_p \cdot \dot{m}_f \cdot \Delta T \tag{2.11.}$$

2.3.2. BLI modelling

In this study to simplify the analysis the inner control volume approach [18],[21] is assumed, this approach only includes in the analysis the propulsor, neglecting the airframe and its wake. The benefit of this method is that it uncouples the airframe and propulsion design, as the drag ingested from the airframe is not included in the calculation. However, to include the performance benefits coming from BLI, the velocity profile of the flow ingested by the propulsor is needed.
This velocity profile at the intake of the propulsor control volume defines the propulsor's momentum drag and hence the benefits accrued from BLI will be related to the reduction in inlet velocity. Based on this premise, the parametric BLI assessment starts by defining

the mass averaged velocity at the inlet station of the propulsor's control volume. For this aim is necessary also to define where the propulsors will be located.

For this work, they are assumed to be embedded and using s-shaped ducts, such that the aircraft drag will not be affected by the propulsor array design. Furthermore, it is assumed that the inlet of the propulsor's control volume is located at the same distance than in the podded case and only the centerline has been assessed. Therefore, the three-dimensional (spanwise) variation of the boundary layer development has been neglected. Analogously to the podded case the pre-compression zone is not considered and the intake height assumed equal to the height of the capture sheet (HCS). In Figure 2.4 is shown the control volume used for the BLI case.

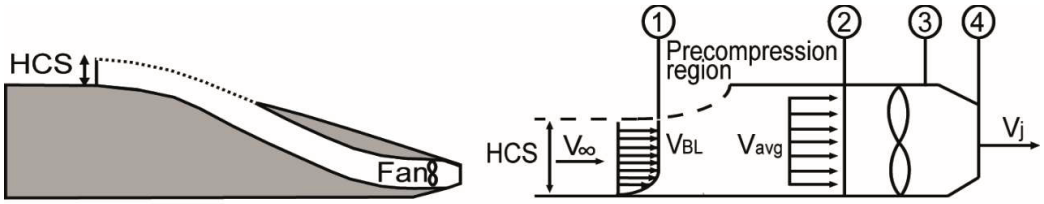

Figure 2.4. Inner control volume for the BLI configuration *[30]*.

For the boundary layer modeling, the airframe is represented as flat plate, then the correlations for turbulent flow are used to describe boundary layer thickness. Three approaches are selected to model the boundary layer: the 5th, the 7th power law and Guo's model [46] this later has been validated for subsonic flow. The velocity profile equation developed by Guo is shown in equation. 2.13.

$$\frac{V}{V_*} = \frac{V_\infty}{V} + \frac{1}{k}\left(ln\xi - 2\pi cos^2\frac{\pi\xi}{2} + \frac{1-\xi^3}{3} \right) \tag{2.13.}$$

$$\xi = \frac{y \cdot V_*/\vartheta}{Re_\delta} \tag{2.14.}$$

Since the propulsor performance tool is 1D the velocity profiles need to be mass averaged and for this task, equation 2.15 is utilized.

$$V_{avg} = \frac{\sum_{i=1}^{n} \dot{m} \cdot V_0}{\sum_{i=1}^{n} \dot{m}} = \frac{\int_0^\delta \left(V_\infty \cdot \left(\frac{y}{\delta}\right)^n \right)^2 \cdot dy}{\int_0^\delta V_\infty \cdot \left(\frac{y}{\delta}\right)^n \cdot dy} = \frac{n+1}{n+2} \cdot V_\infty \tag{2.15.}$$

2.4. Thrust split

In this work, non-homogeneous configurations of thrust distribution have been also evaluated. As presented before, in thrust split (TS) configurations the thrust for a determined operating condition comes from a non-homogeneous propulsion system, which is integrated by a main propulsor (MP) and some secondary propulsors (SP).
For the TS evaluation an adaptation of the parametric code developed was made and different configurations were evaluated to propose an optimum configuration. A comparison of the proposed cases with a case without thrust split in terms of power, diameter and torque required by the fans was done.

2.5. Airframe propulsion integration problems

In this section, different types of integration problems will be evaluated, such as distortions due pressure losses in the intake and fan efficiency. Three different geometries for the duct were studied and an experimental test to calculate the fan efficiency were carried out.

2.5.1. Intake pressure losses modelling

Three different inlet geometries (shown in figure 2.5) were selected to analyze their pressure losses: a rectangular, circular and a combination between both geometries. This selection was based on the parametric duct design presented by Sands [47]. In the results section these three geometries and the parameters used to define them are described. Since at this preliminary design stage the detail design of the intake is unknown, some assumptions to determine its geometry have been taken: the duct height is assumed equal to the fan diameter and the duct width (w) is defined through the geometry ratio (GR). It is important to note that the intake width definition is only used for the pressure losses calculation. In future studies the precompression region needs to be assessed in order to determine the actual shape of the duct and how the flow properties will be affected before and after the intake. For the intake losses calculation three GR are explored 1,1, 1,3 and 1,5. The length of the duct was established taking into account equation 2.16, which is based on the studies carried out by Rodriguez [18], where an optimal duct length is determined based on the airframe centerline chord.

$$L_d = 0{,}0834 \times c \tag{2.16.}$$

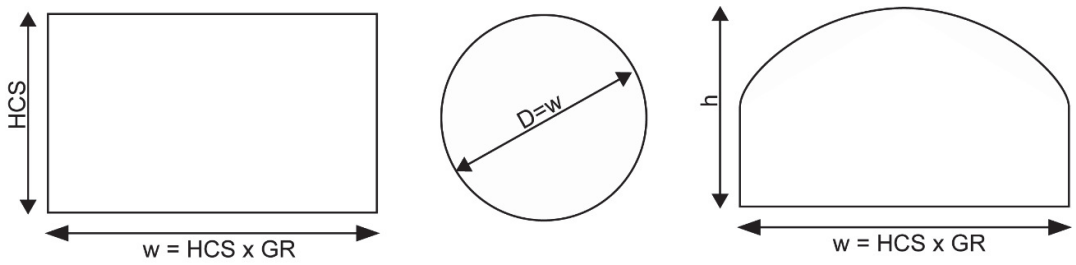

Figure 2.5. Inlet geometries selected.

Equation 2.17 describes the parametric model used, to calculate de total pressure loss trough the duct. This model is selected, as it has been contrasted against experimental results for rectangular ducts and its prediction is good enough for preliminary design [40]. In the present work, the pressure losses will be calculated assuming a friction factor (f) obtained in the Moodys diagram considering fiber carbon as the duct material.

$$\Delta P_{in} = \frac{4 \cdot f \cdot \rho \cdot L_f . V^2}{2\, D_h} \tag{2.17.}$$

$$D_h = \frac{4 \cdot A}{p} \tag{2.18.}$$

2.5.2. Fan efficiency

For the calculation of the fan efficiency, experimental data was used. Temperature, pressure and velocity data were measured at the intake and exit of the fan. The velocities and static air temperature were measured with an anemometer and thermometer, respectively. With this data the total air properties were calculated to obtain the FPR and the in this operating point as shown in equation 2.19, taking into account that the experiment was done at a height of 2800 meters above sea level. For all the data calculated the standard deviation was considered.

$$FPR = \frac{p_{amb2} + \frac{1}{2}\rho \cdot V_j^2}{p_{amb1} + \frac{1}{2}\rho \cdot V_0^2} \tag{2.19.}$$

To calculate the fan efficiency, stage loading and flow coefficient parameters, defined by Dixon [33] were used (equations 1.3,1.4,1.5) . The fan efficiency is defined as the ratio between the real and theoretical stage loading. The ducted fan utilized for this experimental study was a 0.064 m diameter ducted fan [41].

3. RESULTS AND DISCUSSION

This section presents the results obtained with the models previously described. In order to assess a larger spectrum of distributed propulsion configurations, in this analysis three case scenarios have been explored. Each case scenario presents an aircraft with different planform area: Case A: 0,127 (m^2), Case B: 1,27 (m^2) and Case C: 6.35 (m^2). The last case corresponds to a planform area similar to the NASA XB-48 [12]. The assessment of these three cases enables to find out where the technologies aforementioned are suitable.

3.1. BLI Analysis

Figure 3.1 shows a comparison between the boundary layer profiles non dimensionalized for the freestream velocity (x axis), boundary layer thickness (figure a) and for the propulsor diameter (figure b). From the left figure is evident that the 5th power law and Guo's profile capture the boundary layer with similar accuracy. Since Guo's profile is validated against experimental data[46], this latter is selected to model the boundary layer in the distributed propulsion performance assessment. The right diagram has been corrected for the propulsors size, D_f = 0.06 (m), which has been defined for the three cases of analysis based on the smallest size electric ducted fan available in the market [41]. As observed insofar as the boundary layer thickness increases and the fan diameter decreases, the amount of boundary layer ingested is larger and therefore is expected a lower momentum drag at the propulsor inlet improving the benefits of BLI. However, there is a physical limitation to the size reduction as aforementioned. Therefore, in a practical scenario the cases for larger propulsors will be the ones suitable for distributed propulsion with BLI. Table 3.1 show the mass averaged velocities used as inlet velocity conditions for the propulsion control volume in the performance module.

Table 3.1. Mass average velocity for different boundary layer profiles.

Case	Guo's profile	5^{th} power law profile	7^{th} power law profile
A	32,394 (m/s)	32.362 (m/s)	32.471 (m/s)
B	31.136 (m/s)	31.018 (m/s)	31.426 (m/s)
C	30.508 (m/s)	30.348 (m/s)	30.905 (m/s)

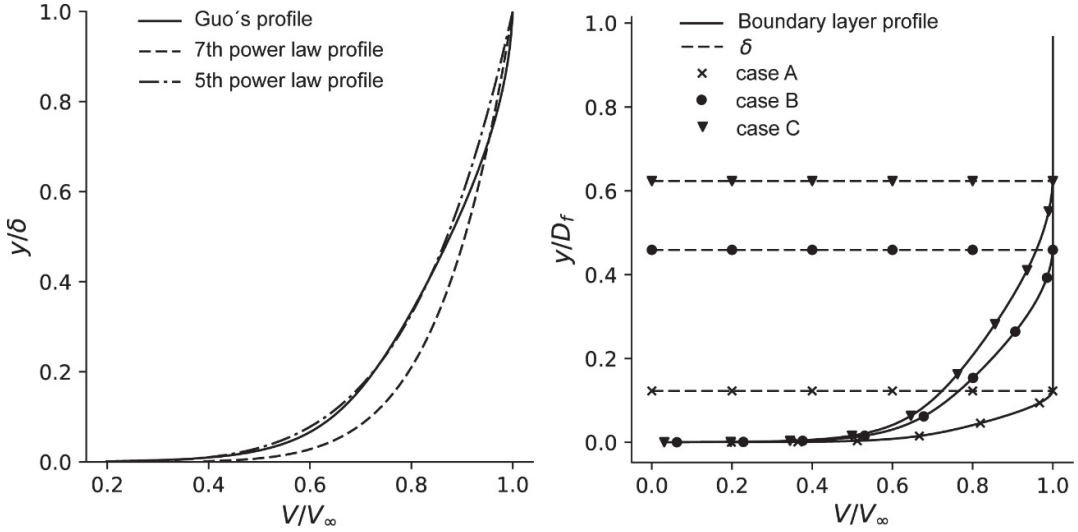

a) Boundary layer profile comparison.

b) Boundary layer profiles non dimensionalized for the smallest propulsor diameter.

Figure 3.1. Boundary layer profiles comparison.

3.2. Airframe integration problems

Firstly, the results of pressure loss in the duct for the different geometries and different Geometry ratio are discusses. Secondly, the experimental results of the fan efficiency are shown.

3.2.1. Intake pressure losses effect

To contrast the validation of the duct pressure loss model developed by Jaurker [40], a duct of 10 m length (reference length for a duct of a commercial airplane) was analyzed. In this analysis the pressure loss was close to 5%, which agrees with duct losses for this sort of designs [18]. The three geometries mentioned in the methodology section and also three different geometry ratios (1,3, 1,5 and 1,7) were considered. Figure 3.2 shows the results corresponding to each configuration. For a GR = 1.3 the mixed geometry presents a pressure loss higher than the other geometries, but for GR= 1.5 and 1.7 the pressure loss is lower, reaching 0.25% for a 0.5 (m) duct length. This is caused by the simplistic model used, where the hydraulic diameter increases when two different geometries are combined (equations 2.17 and 2.18). However, since the importance of this parameter is large in the propulsion performance, this model should be enhanced in future work. The highest pressure loss for the mixed geometry is around 0,5% for a duct length of 0,5 (m). For the present study, according to the dimensions of the aircraft, the

duct length would be approximately 0,033 m according to Rodriguez [18]. These results are interesting as show small values for most of the configurations, which is an advantage in the implementation of embedded ducts in comparison with civil aviation concepts [32]. For the rectangular and circular geometry, the behaviour of pressure losses is similar. The pressure loss decreases while GR increases. The circular geometry presents lower pressure losses for each GR considered comparing with the rectangular geometry, because of the bigger hydraulic diameter.

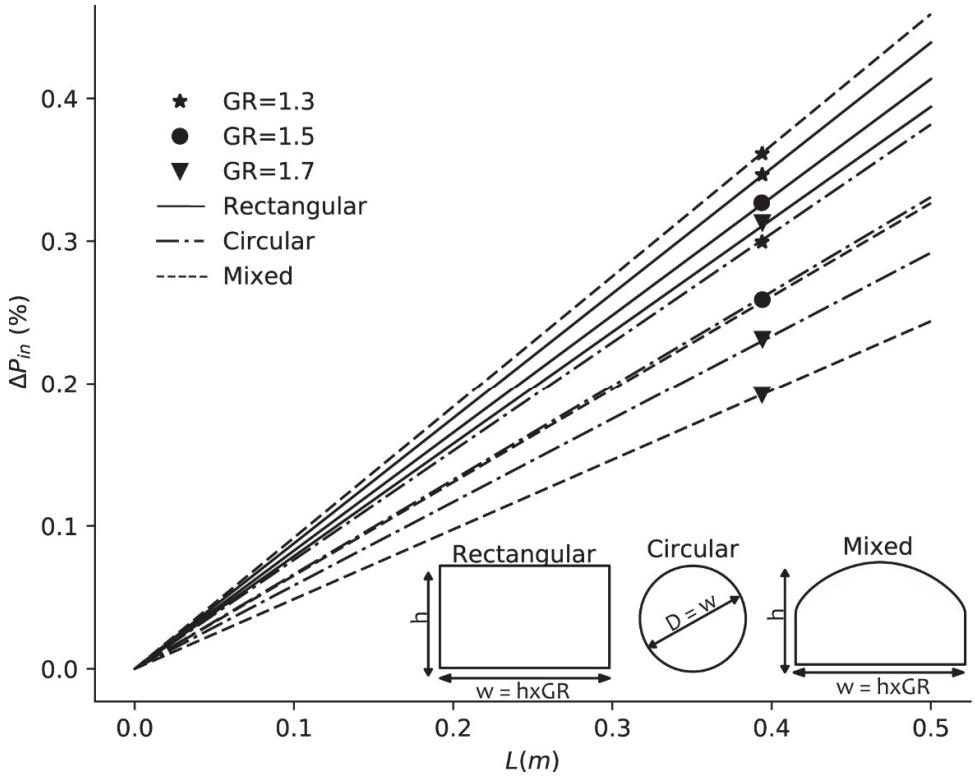

Figure 3.2. Pressure loss for different inlet geometries.

3.2.2. Fan efficiency

To select the operating point to calculate the fan efficiency, two different studies were considered, in which the FPR was around 1,1 and 1,3. The first study carried out by Kerho [5] shows a ducted fan (D= 0.128 m) which efficiency is 70% for a FPR of 1,1. In the second study an aerodynamic design of integrated propulsion-airframe configuration of the hybrid wing body was carried out by Liou [48] in which the FPR equal to 1,3 was determined from the system study.

The fan efficiency was calculated by taking the experimental data measured in the wind tunnel. Where pressure, temperature, and air velocity were measured, at the intake and exit of the fan, obtaining a FPR of 1,1971 with a standard deviation of 0,01624.

This last data was used for the subsequent analysis for the calculation of propulsive efficiency. The experimental results are summarized in table 3.2.

Regarding the isentropic efficiency of the fan, considering BLI, an efficiency of 58% was obtained with a standard deviation of 3%. Which was a comparison between the real stage loading and the theoretical one, according to what is indicated in the theoretical framework section. Like the FPR, the isentropic efficiency obtained was taken as an initial data for subsequent calculations when BLI is considered.

The efficiency given by the manufacturer without considering BLI is 70%, which means that the efficiency decreased 12%. Previous work show a 2% detriment due to BLI [25], [32]. Due to this result, a future work to evaluate the efficiency of the same fan without considering BLI is recommended. The decrease in efficiency happens due to the decrease in the inlet velocity to the propeller due to the BLI, this lower velocity results in a lower mass flow which implies that more work must be done to generate the same thrust. The relationship between power and mass flow can be seen in equation 2.12. The reduction in efficiency could mean that the fan was not operating at its optimum performance point. Therefore, the calculation of this point is left as future work as well.

Table 3.2. Experimental results.

Parameter	Value	Standard deviation
Fan pressure ratio FPR	1,1971	0,01624
Fan temperature ratio	1,1643	0,05762
Theoretical stage loading φ	0,4554	-
Real stage loading φ	0,2630	0,01301
Mass flow coefficient $\emptyset$	1,243	-
Fan efficiency n_f	58%	3%

3.3. BLI analysis

In this section, results for a planform area equal to 3,127 (m^2). This area was chosen based in results obtained for the three scenario cases. Starting with this area, a suitable configuration for five fans with similar diameter of the one tested in the experimental results was determined.

First the results for propulsive efficiency for a comparison between the podded and the BLI case are analyzed.

Secondly, the results of power, torque, diameter and mass flow required by the fans are discussed for the same two cases. Taking as input data the previously calculated parameters.

3.3.1. Propulsive efficiency

Figure 3.3 shows how the propulsive efficiency varies for the podded and a BLI configuration for two different velocity profiles. The results show a slight increase in the propulsive efficiency in the BLI configuration around 0,2% for the different FPR. The tendency of the decrease in the propulsive efficiency while the FPR rises is practically linear up to an FPR of 1,2 which is the considered operation point for the fans in the case studied, obtaining at this point an efficiency of 35% without BLI and 35,2% approximately considering BLI.

This increase in propulsive efficiency is due to the lower intake velocity to the fan. The inverse relationship that exists between intake velocity to fan due to BLI, the velocity at the exit and free stream velocity can be seen in equation 2.16. By implementing BLI, the propulsive efficiency increases. The reason for this behavior is that by decreasing the intake velocity, the available power decreases while the useful power used by the fan remains constant.

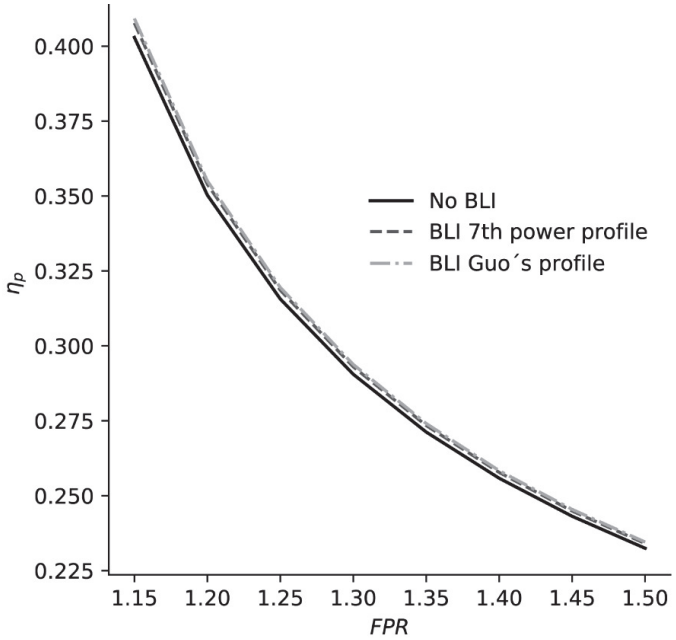

Figure 3.3. Propulsive efficiency.

3.3.2. Power and torque required, Podded and BLI case

Figure 3.4 shows the results of the parametric code for the power and torque required by the fans based on the diameter and mass flow in a range of FPR of 1,15 to 1,5. For higher FPR the power required increases because more energy is needed to produce a higher pressure at the exit of the fan. At the same time the mass flow reduces because for the present calculation the intrinsic net thrust is considered constant. Taking as an example of application 3 fans, the power, and torque required, are 3078 (W) and 0,551 (Nm) respectively for a 0,09756 (m) fan diameter, corresponding to a FPR of 1,2. For the same FPR, in the BLI case, the power and torque required rise to 3681 (W) and 0,5873 (Nm) for a 0,09358 (m) fan diameter, which means an increase in the power required about 19,59% and 6,59% in the torque required. This increase in both, power and torque, is mainly due to the decrease of the fan efficiency as mentioned above. The decrease of the mass flow in the case of BLI is given by the reduction of the intake velocity, which is also reflected in a lower fan diameter required. For 5 and 7 fans, the increase in the power required is about 19,6%. Figure 3.4 shows a FPR of 1,2 for the case of 7 fans, because the size of the fans for this configuration are similar to the fan diameter used in the experimental tests.

The same study was carried out for heights of 4000 and 5000 (m) above the sea level, obtaining an increase in the total power required of 0,3% each 1000 (m) of analysis, while the total torque required increased approximately 1,8% each 1000 (m) of analysis.

The increase in both parameters is due to the change in air characteristics, such as the decrease in its density, temperature and pressure. This decrease in the air properties implies a reduction in the mass flow. Therefore, more power and torque are needed to be able to move the same mass of air that the fan needs to generate the same thrust as at lower altitudes.

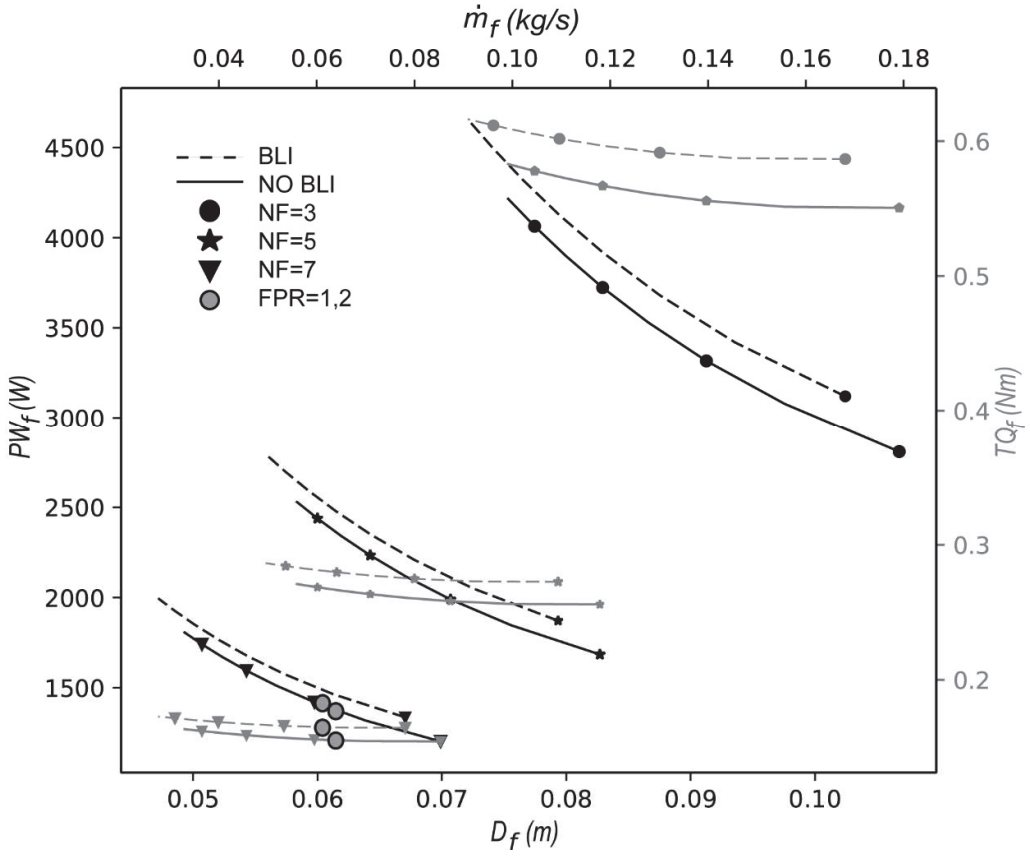

Figure 3.4. Torque and Power vs Diameter and Mass flow required by each fan for a podded case and a BLI configuration.

3.4. Thrust Split evaluation

Figure 3.5 shows the power consumption per fan for 40 % and 60 % TS, for the scenario case C. As observed the case of 60 % TS with 4 secondary propulsors enables the implementation of distributed propulsion with BLI.

For lower drag forces, the fan diameter required decreases less than 0,06 (m) which represents a problem for the acquisition and handling thereof. Figure 3.5 shows the power required by the propellers based on the diameter for a configuration of 40% and 60% of thrust split.

The figure is divided according to the smaller size of a fan found in the market while the realization of the present work (D = 0,064 (m)), and with which the experimental tests were carried out.

For lower drag forces, as the drag considered in the present case of study, thrust split does not represent a benefit because of the size of the propellers. For higher drag forces, a thrust split configuration could represent geometry benefits in terms of the reduction of the diameter size of the secondary propellers; or benefits in terms of the propulsor's weight. In addition, lower fan diameters would represent a higher y to D_f ratio, which is beneficial to increase the propulsive efficiency because of the reduction of the intake velocity due to the BLI.

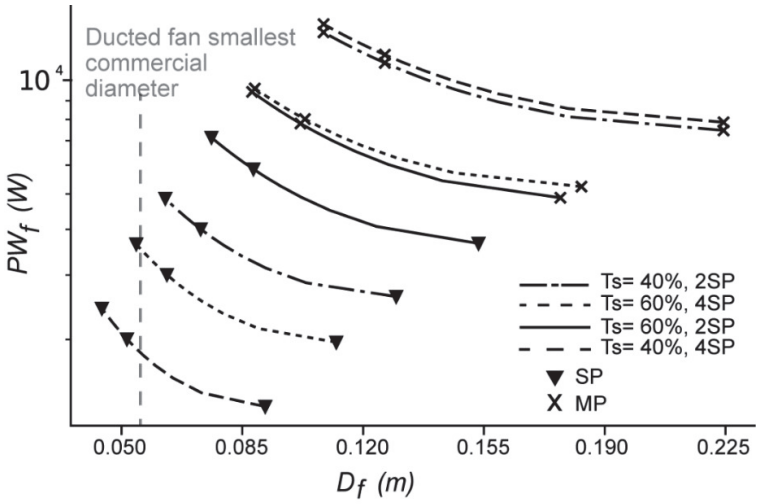

Figure 3.5. Torque and Power vs Diameter and Mass flow required by each fan, TS= 60% for different drag forces.

3.5 Summary

In the present work, for the same type of aircraft, three different planform areas were initially studied. The aircraft was chosen according to the operating conditions stablished for the investigation. In base of these results, a planform area was selected started to be suitable with the fan used in the experimental tests.

At first stage, an analysis of different boundary layer profiles to evaluate their behavior and calculate the mass average velocity for a 0,06 (m) diameter fan was carried out. In this analysis 3 profiles were studied, where the Guo´s profile was selected for later analysis by data obtained in his research. From these results, a study of the propulsive efficiency was done comparing a podded and BLI configuration, obtaining approximately 0,2% of improvement in this efficiency.

At second stage, a duct design was carried out considering three different type of geometries. The duct length (0,034 (m)) was calculated based on the results obtained by Rodriguez [18]. The pressure loss in the duct was analyzed with a 0,5% of loss in the worst case for a 0,5 (m) duct length. From this analysis the lower pressure loss was obtained in the mixed geometry with a GR equal to 1,7. As pressure loss in small ducts does not represent a high power increment in the propulsors, the duct design is not a big challenge.

At third stage, for the fan efficiency calculation, experimental data were taken (pressure, temperature and wind velocity) in a wind tunnel simulating a BLI configuration. From this experimentation, an efficiency of 58% was obtained with a standard deviation of 3%. This efficiency value was used for later calculation of power, torque and diameter required by the propulsors as well as the value obtained from the pressure loss in the duct.

At final stage, the calculation of power, torque and diameter required by the fans for a podded and BLI configuration was carried out. A reduction in power and torque required was expected for the BLI configuration. Despite this, an increase in the power and torque was obtained due to the decrease in fan efficiency, (from 70% to 58% without and with BLI respectively). Which implied that the increase in power was higher than the decrease due to the implementation of BLI. Finally, different TS configurations were analyzed, noting that for small aircraft there is no great benefit since the percentage of ingested boundary layer is relatively small, and its benefit increases while the area of the aircraft increases, maintaining the size of the propulsor.

Due to the decrease in fan efficiency, and the small percentage of the boundary layer ingested, the implementation of BLI in small aircraft does not represent any benefit since the power and torque required increment.

3.6 Future work

Determine the optimum operation point of the ducted fan studied with experimental tests in the wind tunnel. In addition, calculate the fan efficiency without a BLI configuration. With this result, analyze the power and torque required for both configurations (BLI and podded).

CONCLUSIONS

- Distributed propulsion configurations in a BWB UAV for SSM in the Andean region was studied using parametric models. The performance of distributed propulsion was conducted in order to define the suitability of these systems and the benefits that can be achieved by its implementation. Furthermore, BLI and thrust split were explored as technologies to set potential UAV configurations based on lower power consumption, geometrical suitability and propulsive efficiency.
- The methodology implemented enabled to define the space of design for distributed propulsion systems and the sensitivity to main design drivers such as: number of fans, thrust split and airframe size.
- A preliminary configuration of distributed propulsion with seven thrusters was proposed. This number of propellers was taken into account due to the size of the propellers and the space offered by the aircraft studied. The power required for a configuration without BLI and another with BLI was obtained for the case of study for an FPR of 1,2. In the case of the configuration with BLI, there was a decrease in fan efficiency of 12%. Which produced an increase in the required power of 19% and the required torque of 6,59%. Due to this behavior, a future work to study the efficiency of the propeller without considering BLI and find its optimum point of operation is recommended. Regarding the pressures losses in the duct of the propellers, low pressure losses were obtained (0,5% for the most unfavorable case) due to the small length of the duct. For civil aviation, higher pressure losses, about 5%, are expected.
- For the thrust split assessment, different planform areas were evaluated for the same type of aircraft. In small airplanes the TS does not represent any benefit since the secondary fans would have very small diameters which makes its manufacture or acquisition in the market difficult. In the case of large aircraft, which require higher thrust, the TS can generate great benefits since the secondary propellers could ingest a large part of the boundary layer and an increase of propulsive efficiency could be higher, in addition to geometric advantages and weight reduction.

BIBLIOGRAPHIC REFERENCES

[1] SENPLADES, *Plan Nacional Del Buen Vivir.* 2013.

[2] Ministerio del Ambiente del Ecuador, *Polticas y plan estratgico del sistema nacional de reas protegidas del ecuador*. 2007.

[3] Trimble inc., “Trimble ux5. Aerial imaging solution for agriculture agronomic services.” .

[4] Valencia Esteban, Benálcazar Marco, Saá Juan, Mange Nicolás, and Hidalgo Víctor, “Design point analysis of a distributed propulsion system with boundary layer ingestion implemented in UAVs for agriculture in the Andean region.,” presented at the 52nd AIAA/SAE/ASEE Joint Propulsion Conference, Salt Lake City, UT, 2016.

[5] M. Kerho and B. Kramer, “Turboelectric Distributed Propulsion Test Bed Aircraft,” presented at the NASA Aeronautics Research Mission Directorate (ARMD), Rolling Hills Research Corporation, Nov-2013.

[6] E. Valencia, V. Hidalgo, and O. Calle, “Weight and performance methodology of a uav at cruise condition of precision agriculture,” 2017.

[7] R. H. Liebeck, “Design of the blended wing body subsonic transport,” *Journal of Aircraft*, vol. 41, 2004.

[8] D. J. Thompson, J. Feys, M. D. Filewich, S. Abdel-Magid, D. Dalli, and F. Goto, “The Design and Construction of a Blended Wing Body UAV,” presented at the 49th AIAA Aerospace Sciences Meeting including the New Horizons Forum and Aerospace Exposition, Orlando FL, USA, 2011.

[9] E. Valencia, L. Chengyuan, P. Laskaridis, and R. Singh, “An Alternative Configuration for Distributed Propulsion with Boundary Layer Ingestion on a Hybrid Wing Body Airframe,” presented at the ISABE, Busan, Korea, 2013.

[10] M. Armstrong, C. Ross, M. Blackwelder, and K. Rajashekara, “Trade studies for NASA N3-X turboelectric distributed propulsion system electrical power system architecture,” *SAE International Journal of Aerospace,* no. 5(2012-01-2163), 325-336., 2012.

[11] G. Creech, “Back in the air: X-48B resume fligth tests at NASA dryden.,” NASA, USA, 2010.

[12] T. Risch, G. Consentino, C. Regan, M. Kisska, and N. Princen, “X-48B fligth test progress overview,” *AIAA*, 2009.

[13] Wirachman Wisnoe, Firdaus Mohamad, Rizal E. M. Nasir, and Zurriati Mohd Ali, “Experimental results analysis for UiTM BWB baseline-I and baseline II UAV running at 0.1 Mach number,” *International Journal of mechanics*, 2010.

[14] H. J. Shim and S. O. Park, “Low-speed wind-tunnel test results of a BWB-UCAV model,” presented at the 7th Asian-Pacific Conference on Aerospace Technology and Science, 7th APCATS 2013, Sun-moon Lake, Taiwan, 2013.

[15] Y.-H. Jo, K. Chang, D.-J. Sheen, and S. H. Park, “Numerical simulation of aerodynamic characteristics of a BWB UCAV configuration with transition models,” *Int. J. Aeronaut. Spaces Sci.*, 2015.

[16] O. Gur and A. Rosen, “Optimizing Electric Propulsion Systems for Unmanned Aerial Vehicles,” vol. 46, pp. 1340–1353, 2009.

[17] J. L. Felder, H. D. Kim, and G. V. Brown, “Turboelectric distributed propulsion engine cycle analysis for hybrid wing body aircraft.,” presented at the 47th AIAA Aerospace Sciences Meeting, Orlando FL, USA, 2009.
[18] D. L. Rodriguez, “A multidisciplinary optimization method for designing boundary layer ingesting inlets.,” Stanford University, 2001.
[19] R. Kirner, “An investigation into the benefits of distributed propulsion on advanced aircraft configurations,” Cranfield University, Cranfield, 2013.
[20] L. Chengyuan, “Turboelectric Distributed Propulsion System Modelling,” Cranfield University, Cranfield, 2013.
[21] E. Valencia, “Investigation of Propulsion Architectures for Advanced Distributed Propulsion Systems,” Cranfield University, United Kingdom, 2014.
[22] H. D. Kim, “Distributed propulsion vehicles,” presented at the 27th Congress of International Council of the Aeronautical Sciences, France, 2010.
[23] A. Perry, P. Ansell, and M. Kerho, “Aero-Propulsive and Propulsor Cross-Coupling Effects on a Distributed Propulsion System,” presented at the AIAA SciTech Forum, Kissimmee, Florida, 2018.
[24] B. Blumenthal, A. Elmiligui, K. Geiselhart, R. Campbell, M. Maughmer, and S. Schmitz, “Computational Investigation of a Boundary-Layer Ingesting Propulsion System for the Common Research Model,” presented at the 46th AIAA Fluid Dynamics Conference, Washington D.C., 2016.
[25] A. P. Plas *et al.*, “Performance of a boundary layer ingesting (BLI) propulsion system,” presented at the 45th AIAA Aerospace Sciences Meeting and Exhibit, Reno, Nevada, 2007.
[26] C. Goldberg, D. Nalianda, D. MacManus, P. Pilidis, and J. Felder, “Installed Performance Assessment of a Boundary Layer Ingesting Distributed Propulsion System at Design Point,” presented at the 52nd AIAA/SAE/ASEE Joint Propulsion Conference, Salt Lake City, UT, 2016.
[27] A. Uranga *et al.*, “Boundary Layer Ingestion Benefit of the D8 Transport Aircraft,” *AIAA Journal*, Sep. 2017.
[28] ONERA, “Boundary layer.” [Online]. Available: https://www.onera.fr/en/site-index/boundary-layer.html.
[29] E. Valencia, D. Nalianda, P. Laskaridis, and R. Singh, “Methodology to assess the performance of an aircraft concept with distributed propulsion and boundary layer ingestion using a parametric approach,” *Proceedings of the Institution of Mechanical Engineers, Part G: Journal of Aerospace Engineering*, Nov. 2014.
[30] E. Valencia, J. M. Saá, V. Alulema, and V. Hidalgo, “Parametric study of aerodynamic integration issues in highly coupled Blended Wing Body configurations implemented in UAVs,” 2017.
[31] L. Bertola, “Cryogenic applications for visionary aircraft concepts,” Dec-2015. [Online]. Available: http://blogs.nottingham.ac.uk/innovate/2015/12/18/cryogenic-systems-for-aircraft/.
[32] E. Valencia, C. Liu, D. Nalianda, P. Laskaridis, G. Iain, and R. Singh, “Methodology for the assessment of distributed propulsion configurations with boundary layer ingestion using the discretized miller approach.,” *IREASE*, 2017.

[33] S. L. Dixon and C. A. Hall, *Fluid Mechanics and Thermodynamics of Turbomachinery*, 7th ed. Elsevier, 2014.
[34] V. J. Fidalgo, C. Hall, and Y. Collin, “A study of fan-distortion interaction within the nasa rotor 67 transonic stage.,” *J. Turbomach*, 2012.
[35] E. Valencia, V. Hidalgo, P. Laskaridis, D. Nalianda, R. Singh, and L. Chengyuan, “Design Point Analysis of an Hybrid Fuel Cell Gas Turbine Cycle for Advanced Distributed Propulsion Systems,” presented at the 51st AIAA/SAE/ASEE Joint Propulsion Conference, AIAA Propulsion and Energy Forum, (AIAA 2015-3802), Orlando, FL, 2015.
[36] W. Schröder, “Prediction of the Turbulent Flow Field Around a Ducted Axial Fan,” Jun-2015. .
[37] S. A. Gorton, L. Owens, J. Luther, B. Allan, and E. Schuster, “Active flow control on a boundary layer ingesting inlet,” presented at the 42nd AIAA Aerospace Sciences Meeting and Exhibit, Reno, Nevada, 2004.
[38] M. Rein, S. Koch, and M. Rutten, “Experimental Investigations on the Influence of Ingesting B.L. into a Diverterless S-Duct Intake,” presented at the 52nd Aerospace Sciences Meeting, National Harbor, Maryland, USA, 2014.
[39] E. M. Sparrow, J. P. Abraham, and W. J. Minkowycz, “Flow separation in a diverging conical duct: Effect of Reynolds number and divergence angle,” *International Journal of Heat and Mass Transfer*, 2009.
[40] A. R. Jaurker, J. S. Saini, and B. K. Gandhi, “Heat transfer and friction characteristics of rectangular solar air heater duct using rib-grooved artificial roughness.,” 2005.
[41] QX -Motor, “QX-Motor 64mm 5 Blades Ducted Fan With 4300KV 3-4S QF2822 Brushless Motor,” 2017. .
[42] Dirección General de Aciación Civil, *Resolución 251-2015*. 2015.
[43] J. Gundlach, *Designing unmanned aircraft systems: A comprehensive approach.* American Institute of Aeronautics and Astronautics., 2012.
[44] RC Turbines, “Edf ducted fans,” 2016. .
[45] H. I. . Saravanamuttoo, G. F. C. Rogers, and H. Cohen, *Gas turbine theory*. New York, USA: Prentice Hall, 2001.
[46] J. Guo, P. Y. Julien, and R. N. Meroney, “Modified log–wake law for zero-pressure-gradient turbulent boundary layers,” *Journal of Hydraulic Research*, vol. 43, 2005.
[47] J. S. Sands, J. C. Gladin, B. K. Kestner, and D. N. Mavris, “Hybrid Wing Body Engine Cycle Design Exploration for Boundary Layer Ingesting (BLI) Propulsion Systems Under Design Uncertainty,” presented at the AIAA/ASME/SAE/ASEE Joint Propulsion Conference & Exhibit, Atlanta, Georgia., 2012.
[48] M.-F. Liou, K. Hyoungjin, L. ByungJoon, and L. Meng- Sing, “Aerodynamic Design of Integrated Propulsion-Airframe Configuration of the Hybrid Wingbody,” presented at the 35th AIAA Applied Aerodynamics Conference, AIAA AVIATION Forum, (AIAA 2017-3411), Denver, Colorado, 2017.

APPENDIXES

APPENDIX I

Equipment utilized in the experimental test.

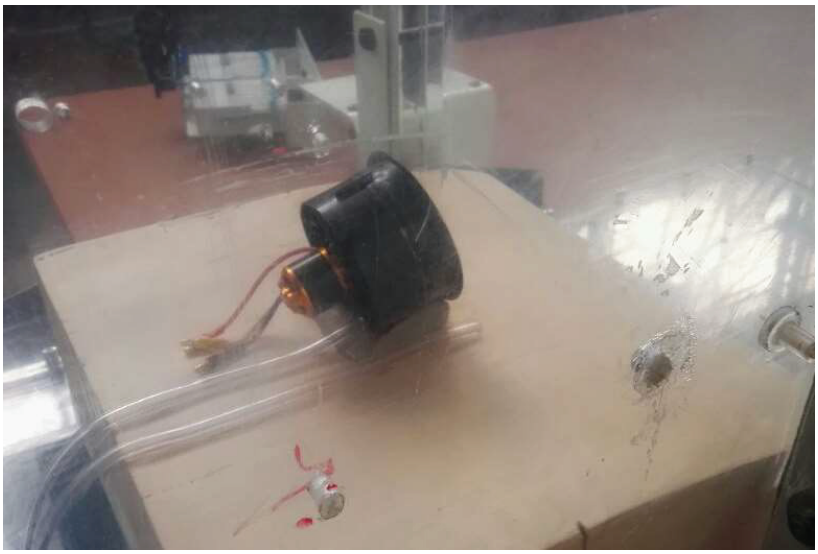

Figure A.1. Ducted fan.

Figure A.2. Ducted fan.

Figure A.3. Wind tunnel.

APPENDIX II

PARAMETRIC CODES DEVELOPED

Code developed adapted for TS configuration

```
%%%%%%%%%%%%%%%%%%%%%%%%%%%%%%%%%%%%%%%%%%%%%%%%%%%%%%%%%%%%%%%%%%%%%%%%
% Airframe coefficient
%%%%%%%%%%%%%%%%%%%%%%%%%%%%%%%%%%%%%%%%%%%%%%%%%%%%%%%%%%%%%%%%%%%%%%%%

CL= 0.5 Lift coefficient
CDo=.00842 Zero lift drag coefficient
S=1.27%input('Input the reference area for the analysis: ');
AR=3.85%input('Input the Aspect Ratio for the analysis: ');
e=.685%input('Input the span efficiency for the analysis: ');

%%%%%%%%%%%%%%%%%%%%%%%%%%%%%%%%%%%%%%%%%%%%%%%%%%%%%%%%%%%%%%%%%%%%%%%%
% Air properties
%%%%%%%%%%%%%%%%%%%%%%%%%%%%%%%%%%%%%%%%%%%%%%%%%%%%%%%%%%%%%%%%%%%%%%%%
Cp=1000;  % Constant Pressure Heat Capacity for cold air
r=1.4;  % Ratio of Specific Heats for Air
R=287;  % Gas Constant for air

%%%%%%%%%%%%%%%%%%%%%%%%%%%%%%%%%%%%%%%%%%%%%%%%%%%%%%%%%%%%%%%%%%%%%%%%
% Numeric constant
%%%%%%%%%%%%%%%%%%%%%%%%%%%%%%%%%%%%%%%%%%%%%%%%%%%%%%%%%%%%%%%%%%%%%%%%
PI=3.1415926;

%%%%%%%%%%%%%%%%%%%%%%%%%%%%%%%%%%%%%%%%%%%%%%%%%%%%%%%%%%%%%%%%%%%%%%%%
% Aderodynamic coefficient calculation
%%%%%%%%%%%%%%%%%%%%%%%%%%%%%%%%%%%%%%%%%%%%%%%%%%%%%%%%%%%%%%%%%%%%%%%%

CLbestLD=(3*CDo*pi*AR*e)^(1/2)
CDbestLD=CDo+((CLbestLD^2)/(pi*AR*e))

%%%%%%%%%%%%%%%%%%%%%%%%%%%%%%%%%%%%%%%%%%%%%%%%%%%%%%%%%%%%%%%%%%%%%%%%
% Design Point Parameters
%%%%%%%%%%%%%%%%%%%%%%%%%%%%%%%%%%%%%%%%%%%%%%%%%%%%%%%%%%%%%%%%%%%%%%%%
%
Vtip_c=0.15*12000*2*PI/60;

HubtoTipRatio=0.056;

Efffan=0.68;  % Fan Efficiency
H=3000;  % Flight Height At Fan Design Point

%%%%%%%%%%%%%%%%%%%%%%%%%%%%%%%%%%%%%%%%%%%%%%%%%%%%%%%%%%%%%%%%%%%%%%%%
% Calculate the ambient conditions at Fan Design Point
%%%%%%%%%%%%%%%%%%%%%%%%%%%%%%%%%%%%%%%%%%%%%%%%%%%%%%%%%%%%%%%%%%%%%%%%
if H < 11000
    t_amb = 288.15-0.0065*H;
    p_amb = 101325*(1-0.0000226*H)^(5.256);  %Pa
    ro_amb = 1.226*(1-0.0000226*H)^(5.256);  % kg/m^3
    a_amb = (r*R*t_amb)^0.5;            % m/s
```

```
else
    t_amb = 271.15-56.5;   % K
    p_amb = 22557.74*exp(-(H-11000)/6341.33);
    ro_amb = 0.363*exp(-(H-11000)/6341.33) ;
    a_amb = (r*R*t_amb)^0.5;
end
V0=30.533; % Mass average velocity
   Tamb = t_amb * (1+Mdesign^2*(r-1)/2);  % Total ambient temperature
   Pamb = p_amb * (1+Mdesign^2*(r-1)/2)^(r/(r-1));  % total ambient
pressure ecuaciones de gases compresibles

D=CDbestLD*(1/2)*ro_amb*(V0^2)*S %Drag at cruise
THR=D;  % Total Thrust Required At Fan Design Point assumed as 1/5 of the
take-off thrust

THRF=THR/NF;  % Thrust Required for Each Fan

%%%%%%%%%%%%%%%%%%%%%%%%%%%%%%%%%%%%%%%%%%%%%%%%%%%%%%%%%%%%%%%%%%%%%%%
% Design Point Calculations
%%%%%%%%%%%%%%%%%%%%%%%%%%%%%%%%%%%%%%%%%%%%%%%%%%%%%%%%%%%%%%%%%%%%%%%

%%%%%%%%%%%%%%
% Intake
%%%%%%%%%%%%%%
P1=Pamb; %taken from Felder11:AE
P2=P1*(1-PL);  % 1% Pressure Loss for Intake
T1=Tamb;
T2=T1;
% Calculate the inlet conditions and area of the fan
M2=0.1;%%%%%%%%%%%%%%%%%%%%%%%%%%%%%%%%%%%%%%%%%%%%%%%%%%%%%%%%%%%%%%%How was
determined
t2=T2*(1+((r-1)/2)*M2^2) %t2=T2/(1+(M2)^2*(r-1)/2); %t2 temp estática
p2= P2*(1+((r-1)/2)*M2^2)^(r/(r-1))% tomado de Cengel %p2=P2/(((M2)^2*(r-
1)/2+1)^(r/(r-1)));
den2=p2/(R*t2);
a2=(r*R*t2)^(1/2);
V2=M2*a2;

%%%%%%%%%%%%%%
% Fan
%%%%%%%%%%%%%%
P3=P2*PRfan;
T3ideal=(PRfan^((r-1)/r))*T2;
T3=(T3ideal-T2)/Efffan+T2;

%%%%%%%%%%%%%%
% Nozzle
%%%%%%%%%%%%%%
T4=T3;
P4=P3*(1-PL);  % Pressure Loss for By Pass Duct and nozzle(Due to
friction in weted area)
p4=p_amb;  % Always Fully Expanded at Design Point
Me=(((P4/p4)^((r-1)/r)-1)/((r-1)/2))^(1/2) % Exit Mach No. Should be less
than 1 at design point

if (Me<1)  % Check Whether The Nozzle is Chocked
    Me=Me;
else
    Me=1;
```

```
end

p4=P4/((Me^2*(r-1)/2+1)^(r/(r-1)));
t4=T4/(1+(r-1)/2*(Me)^2);
a4=(r*R*t4)^(1/2);  % Exit Sound Speed
V4=Me*a4  % Exit flow velocity
Vj=V4  % Exit jet velocity

% If Nozzle is chocked at design point, the exit area need to be
calculated using iterations
if (Me==1)
    A4H=10;
    A4L=0;
    A4G=(A4H+A4L)/2;
    k=1;
    while (k==1)
        W=(THRF-(p4-p_amb)*A4G)/(Vj-V0);  % Mass Flow
        den=p4/(R*t4);  % Exit Flow Density
        A4Cal=W/(den*Vj);  % Nozzle Exit Area at Design Point
        DiffA4=abs(A4G-A4Cal);
        if (DiffA4<0.000001)
            A4design=A4G;
            W=(THRF-(p4-p_amb)*A4design)/(Vj-V0);  % Mass Flow
            k=0;
        else
            if (A4G<A4Cal)
                A4L=A4G;
                A4G=(A4H+A4L)/2;
            else
                A4H=A4G;
                A4G=(A4H+A4L)/2;
            end
            k=1;
        end
    end
else
    W=THRF/(Vj-V0);  % Mass Flow per fan
    den=p4/(R*t4);  % Exit Flow Density
    A4design=W/(den*Vj);  % Nozzle Exit Area at Design Point
end
A4design;
A2design=W/(den2*V2);
D2=(A2design*4/(PI*(1-0.056^2)))^0.5
D4=(A4design*4/(PI*(1-0.056^2)))^0.5
Vtip=Vtip_c*(T2/288.15)^(1/2)
Nfan=Vtip*2/D2 %[rd/s]

%%%%%%%%%%%%%
% Performance
%%%%%%%%%%%%%
P0=101325;  % standard total pressure at sea level
T0=288.15;  % standard total temperature at sea level
delta=P2/P0;  % the ratio of fan inlet total pressure vs. the standard
one at sea level
theta=T2/T0;  % the ratio of fan inlet total temperature vs. the standard
one at sea level
Powerfan=Cp*W*(T3-T2)  % Power Required by Each Fan
MassFlowfan=W  % Mass Flow for each fan
MassFlowtotal=MassFlowfan*NF  % total mass flow
```

```
Torqfan=Powerfan/(Nfan)  % Fan Torque
Powertotal=Powerfan*NF % total fan power
%Propeff=(THRF*V0)/(0.5*W*(Vj^2-V0^2));  % propulsive effectiveness
Propeff=(2)/(1+(Vj/V0));  % propulsive effectiveness
D2design=(A2design*4/(PI*(1-0.056^2)))^0.5;  % fan inlet diameter
FN_cr_emb_tot=THR;
  %Xn=den*Vj*(Vj-V0)*(PI*(0.09/2)^2)
```

Boundary profile assessment and duct design code

```
%%%%%%%%%%%%%%%%%%%%%%%%%%%%%%%%%%%%%%%%
%Initial parameters.
%%%%%%%%%%%%%%%%%%%%%%%%%%%%%%%%%%%%%%%%

w=0.07; %Duct Width
AR=1.5; %Aspect ratio
h0=w*AR;%Duct Height
L=0.5 %Duct lenght
Ld=[0:0.01:L];
ro_amb=0.8477 %Air property

%%%%%%%%%%%%%%%%%%%%%%%%%%%%%%%%%%%%%%%%
%Duct characteristics calculation
%%%%%%%%%%%%%%%%%%%%%%%%%%%%%%%%%%%%%%%%

Dhr=(2*w*h0)/(w+h0); %Rectangular hydraulic diameter
Dhc=w %Circular hydraulic diameter

%Area for Sands geometry
A0=AR*((h0^2)/2+(pi*h0^2)/8);

%Perimeter for mixed geometry
pS=pi*(3*(w+h0)-((3*w+h0)*(w+3*h0))^(1/2))

DhS=4*A0/pS %Mixed hydraulic diameter

%%%%%%%%%%%%%%%%%%%%%%%%%%%%%%%%%%%%%%%%
%Boundary profile evaluation
%%%%%%%%%%%%%%%%%%%%%%%%%%%%%%%%%%%%%%%%

U= 32.85477; %m/s
Re=2016256.095;
C=0.027/(Re^(1/7));
uast=U*(C/2)^(1/2);
k=0.4;
PI=0.7577;
d=0.027394;
y=[0.00001:0.00001:d];
yn=ones(size(y));
y2=[d:0.00001:w];
yn2=ones(size(y2));
p_amb = 7.0058e+04;
f1=0.04 %Moodys diagram


a=zeros(length(y2));
a=a(1,:);
a(1,:)=U;
```

```
%Guo’s profile
u=(U+(uast/k)*(log(y/d)-2*PI*(cos((pi*y)/(2*d))).^2+(1-((y/d).^2))/3))/U;


%7th power law
n=7
u1=(y/d).^(1/n);
u1t=[u1 a];
u5=(y/d).^(1/5);
u5t=[u5 a];

%Promedios másicos
prom7th=(n+1)*U/(n+2);
promGuo=sum((u.^2))*U/sum(u);
prom5th=(5+1)*U/(5+2);

%Promedio total
prom7thTotal=mean([prom7th*yn U*yn2]);
promGuoTotal=mean([promGuo*yn,U*yn2]);
prom5thTotal=mean([prom5th*yn U*yn2]);

%%%%Diseño del ducto%%%%

%Experimental
AP3r=(f1*4*ro_amb*Ld*(prom7thTotal^2))/(2*Dhr);
AP3c=(f1*4*ro_amb*Ld*(prom7thTotal^2))/(2*Dhc);
%AP3cu=(f1*4*ro_amb*Ld*(prom7thTotal^2))/(2*Dhcu);
AP3S=(f1*4*ro_amb*Ld*(prom7thTotal^2))/(2*DhS);

PressureLossAP3r=AP3r*100/p_amb
PressureLossAP3c=AP3c*100/p_amb
%PressureLossAP3cu=AP3cu*100/p_amb
PressureLossAPD=APD*100/p_amb
PressureLossAP3S=AP3S*100/p_amb
```